Volume 203, Number 1, July 2018

ISSN 1047-8477

Journal of Structural Biology

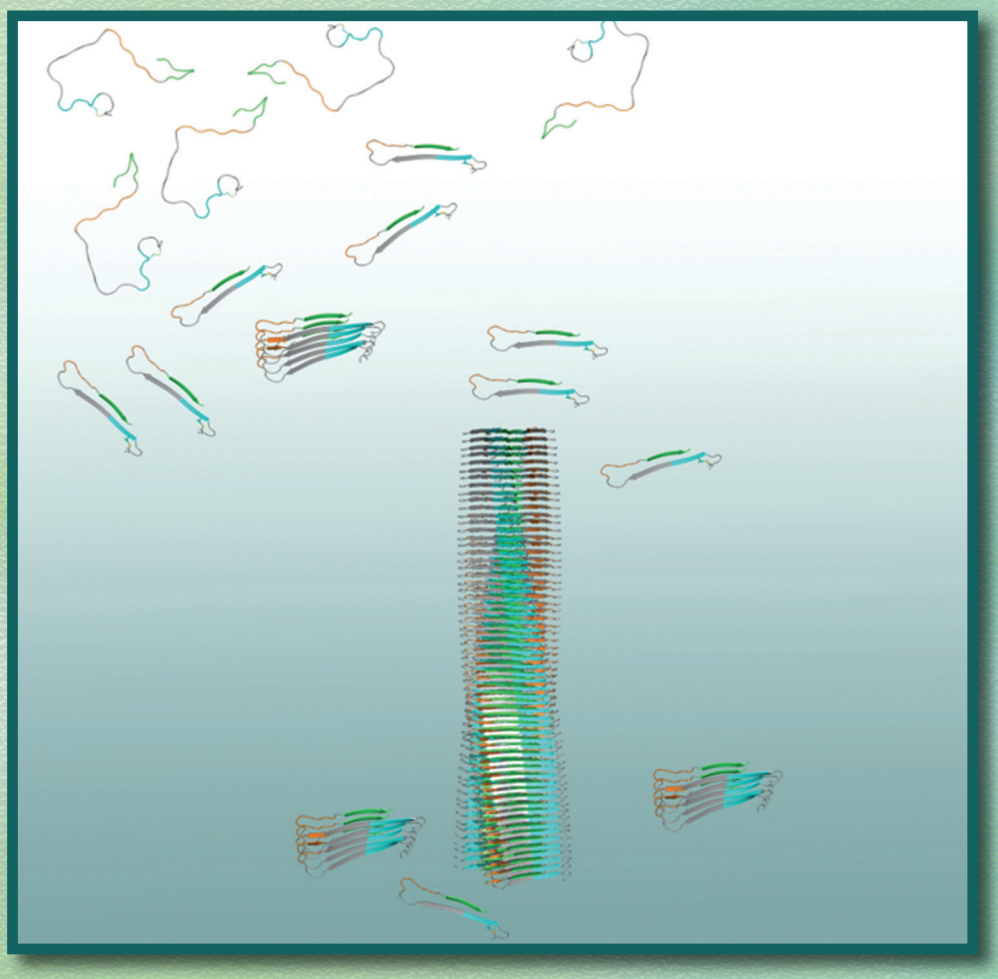

Available online at www.sciencedirect.com

ScienceDirect

Journal of Structural Biology 203 (2018) 27–36

Contents lists available at ScienceDirect

Journal of Structural Biology

journal homepage: www.elsevier.com/locate/yjsbi

αCGRP, another amyloidogenic member of the CGRP family

Paraskevi L. Tsiolaki[a], Georgia I. Nasi[a], Fotis A. Baltoumas[a], Nikolaos N. Louros[a,1], Vassiliki Magafa[b], Stavros J. Hamodrakas[a], Vassiliki A. Iconomidou[a,*]

[a] Section of Cell Biology and Biophysics, Department of Biology, School of Sciences, National and Kapodistrian University of Athens, Panepistimiopolis, Athens 157 01, Greece

[b] Department of Pharmacy, University of Patras, Patras 26504, Greece

ARTICLE INFO

Keywords:
αCGRP
Type 2 diabetes
CGRP family
'Aggregation-prone' peptide
Aggregation assays

ABSTRACT

The Calcitonin-gene related peptide (CGRP) family is a group of peptide hormones, which consists of IAPP, calcitonin, adrenomedullin, intermedin, αCGRP and βCGRP. IAPP and calcitonin have been extensively associated with the formation of amyloid fibrils, causing Type 2 Diabetes and Medullary Thyroid Carcinoma, respectively. In contrast, the potential amyloidogenic properties of αCGRP still remain unexplored, although experimental trials have indicated its presence in deposits, associated with the aforementioned disorders. Therefore, in this work, we investigated the amyloidogenic profile of αCGRP, a 37-residue-long peptide hormone, utilizing both biophysical experimental techniques and Molecular Dynamics simulations. These efforts unravel a novel amyloidogenic member of the CGRP family and provide insights into the mechanism underlying the αCGRP polymerization.

1. Introduction

An important area that is receiving renewed interest is concerned with protein aggregation, since a great number of unrelated, 'prone-to-aggregate' proteins have been identified as causative agents of several devastating clinical disorders (Sipe et al., 2016). Highly ordered protein aggregates, the so-called amyloids, are deposited intra- and/or extracellularly in organs or tissues, by adopting the distinct amyloid architecture (Ashkenazi et al., 1967; Eichner and Radford, 2011; Sunde and Blake, 1997). The association of amyloids with pathologies, such as the Alzheimer's Disease, Parkinson's Disease, Type 2 Diabetes (T2D) or Amyotrophic lateral sclerosis (ALS), has motivated researchers to thoroughly study these abnormal depositions, using a number of *in vitro* biophysical techniques. Thus, *in vitro* studies of several peptides and proteins have shown that, under appropriate conditions, amyloid formation may be an intrinsic attribute of all known soluble proteins (Chiti and Dobson, 2006; Dobson, 1999; Uversky and Fink, 2004).

Human Calcitonin Gene Related Peptide family (or "the CGRP family" or "the calcitonin (CT)/CGRP family" or "the CGRP superfamily") is a group of six (6) conserved peptide hormones that regulate a diverse range of bodily functions (Muff et al., 1995). Namely, calcitonin is an important component of the calcium – phosphorus regulation (Copp and Cheney, 1962), islet amyloid polypeptide (IAPP) is the modulator of glucose metabolism (Roberts et al., 1989), adrenomedullin and intermedin are peptide hormones related to the fine tuning of cardiovascular homeostasis (Lopez and Martinez, 2002), and finally, α and β CGRP, two forms of the Calcitonin Gene Related Peptide (CGRP), possess a wide variety of biological effects both in the brain and in peripheral tissues (Rosenfeld et al., 1992). The receptors of all CGRP family members are formed by similar combinations of two G-protein coupled receptors (GPCRs), namely, the Calcitonin and Calcitonin-like receptors, with three receptor activity-modifying proteins (RAMP 1 to 3) (McLatchie et al., 1998; Poyner et al., 2002), although sequence homology among the members of this family ranges between 20 and 50% (Wimalawansa, 1997) (Fig. S1). Striking, but common features of all CGRP family members also include the N-terminal amino acid ring structure, formed by a single disulfide bridge and the amidated C-terminus (Poyner et al., 2002) (Fig. 1). In addition, the high sequence conservation of both N- and C-terminal regions dictates distinct receptor binding epitopes that all members of this family possess (Poyner

Abbreviations: CGRP, Calcitonin Gene Related Peptide; CT, calcitonin; IAPP, islet amyloid polypeptide; GPCR, G-Protein Coupled Receptor; RAMP, Receptor Activity Modifying Protein; T2D, Type 2 Diabetes; MTC, Medullary Thyroid Carcinoma; MD, Molecular Dynamics; CD, Circular Dichroism; CNS, Central Nervous System; NMR, Nuclear Magnetic Resonance; RMSD, Root mean square deviation; RMSF, Root mean square fluctuation

* Corresponding author.
E-mail addresses: etsiolaki@biol.uoa.gr (P.L. Tsiolaki), gnasi@biol.uoa.gr (G.I. Nasi), fbaltoumas@biol.uoa.gr (F.A. Baltoumas), nlouros@biol.uoa.gr (N.N. Louros), magafa@upatras.gr (V. Magafa), shamodr@biol.uoa.gr (S.J. Hamodrakas), veconom@biol.uoa.gr (V.A. Iconomidou).
[1] Present Address: VIB Switch Laboratory, Department of Molecular Cellular and Molecular Medicine, VIB-KU Leuven, B-3000 Leuven, Belgium.

https://doi.org/10.1016/j.jsb.2018.02.008
Received 2 November 2017; Received in revised form 26 January 2018; Accepted 28 February 2018
Available online 01 March 2018

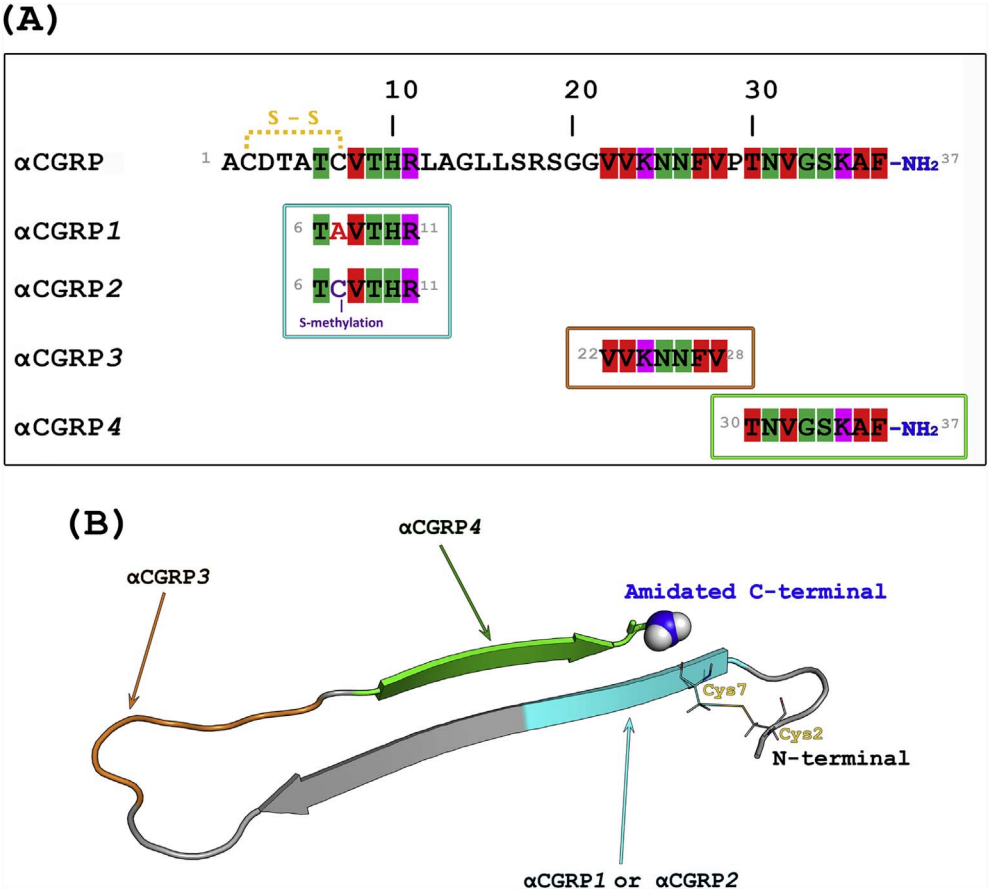

Fig. 1. Amino acid sequence and a model structure of misfolded human αCGRP. (A) The polypeptide sequence normally consists of 37 amino acid residues, having a disulfide bond between the residues Cys-2 and Cys-7 and an amidated C-terminal. Predicted 'aggregation-prone' segments (See), are shown in cyan (^{6}TCVTHR^{11}), orange (^{22}VVKNNFV^{28}), and green (^{30}TNVGSKAF^{37}), respectively, and are annotated according to their physicochemical properties, using the Clustal Omega color code (Sievers et al., 2011). The dashed yellow line points out the existing disulfide bond. (B) A cartoon representation of the misfolded monomer structure of αCGRP, based on the αCGRP sequence similarity with hIAPP (See). Each misfolded monomer adopts a β-strand – loop – β-strand (U-bend) fold. The first β-strand is formed by residues in the 6–18 region, while the second strand involves the 29–37 region. A disulfide bond is formed between the Cys-2 and Cys-7 side chains and the C-termini are amidated. The disulfide bridge is shown in sticks, whereas the amidated C-terminal is presented in spheres. Coloured regions in cyan, orange and green, illustrate the spatial position of αCGRP1 or 2, αCGRP3 and αCGRP4 'aggregation-prone' segments, respectively. (For interpretation of the references to color in this figure legend, the reader is referred to the web version of this article.)

et al., 1993).

Human α Calcitonin gene-related peptide (αCGRP), encoded by the calcitonin gene (CALCA gene), is a 37-residue long neuropeptide and is the most abundant form of CGRP (Amara et al., 1985) (Fig. 1). Conservation of αCGRP across different species (23 of 37 identical residues in mammals) indicates its evolutionary conservation (Ogoshi et al., 2006). Tissue specificity splicing events of the RNA transcripts from the CALCA gene indicate that αCGRP is the predominant product expressed in the Central Nervous System (CNS) (Amara et al., 1982). Although the mechanisms of αCGRP-mediated intracellular signaling are still unclear, due to the peptide's function complexity, it is well-established that αCGRP is a potent vasodilator (Vega and Avila, 2010), and that it is implicated in the regulation of blood pressure (Portaluppi et al., 1993), in cardiovascular homeostasis (Preibisz, 1993), in migraine (Doods et al., 2000) or in pain pathways (Brain and Grant, 2004).

Overall, the members of the CGRP family share the same structural characteristics with other peptide hormones (Kaiser and Kezdy, 1987). Interestingly, both calcitonin (Andreotti et al., 2006) and IAPP (Nanga et al., 2011) were found to adopt an amphiphilic α-helical conformation under normal circumstances, despite their general structural differences, such as the length of the helix or the number and distribution of polar residues. In the light of current knowledge, there are no available crystal structures of αCGRP, even though a number of Nuclear Magnetic Resonance (NMR) and Circular Dichroism (CD) studies attempted to define its conformation (Breeze et al., 1991; Manning, 1989). Three distinct epitopes are confirmed in a 1:1 TFE/water solution (Russell et al., 2014); a N-terminal domain, featuring a ring-like structure and consisting of residues 1–7, a central α-helix with amphiphilic properties between residues 8–18 and an unstructured C-terminal domain, forming the extracellular binding epitope of the molecule with its receptor (Poyner et al., 1999). The central domain between residues 19–28 also displays turn-like properties and was found to be crucial for the molecule's binding affinity, acting, more or less, as a hinge domain (Conner et al., 2002).

The CGRP family has been strongly associated with the formation of ordered protein aggregates, since IAPP and calcitonin were both found as major peptide constituents of T2D (Westermark et al., 1986) and Medullary Thyroid Carcinoma (MTC) (Hazard et al., 1959), respectively. Simultaneously, *in vitro* studies have shown that 'aggregation-prone' segments, covering different functional domains of the aforementioned peptide hormones, exhibit high amyloidogenic potency. More specifically, it has been proved that almost the entire mature polypeptide chain of IAPP displays amyloid-like properties (Fox et al., 2010), whereas in the case of calcitonin segments ^{6}TCMLGT^{11} (Iconomidou et al., 2013) and ^{15}DFNKF^{19} (Reches et al., 2002) contain the key information of polymerization.

In view of the well-established calcitonin and IAPP amyloidogenicity, we investigated αCGRP aggregation properties, utilizing both *in vitro* aggregation assays and Molecular Dynamics (MD) simulations. Additional aggregation studies were performed on several αCGRP peptide fragments, trying to trace fibril-forming segments hidden in the αCGRP polypeptide chain. In this study, we unravel a novel amyloidogenic member of the CGRP family, namely αCGRP, and we try to give a possible explanation on its aggregation properties, by discussing the implications of αCGRP amyloidogenicity in several pathologies.

2. Materials and methods

2.1. Computational sequence analysis of human αCGRP

A secondary structure analysis of mature αCGRP sequence (Uniprot AC: P06881) was performed using SecStr (Hamodrakas, 1988), a consensus predictor available at http://athina.biol.uoa.gr/SecStr/. A joint secondary structure prediction histogram is presented in

Supplementary Fig. S2. The use of the consensus secondary structure prediction algorithm SecStr (Hamodrakas, 1988) suggests a possible helix for residues 8–18 (at least three methods out of six) and a region with turn-like properties between residues 28–35 (at least three methods out of six), supporting previous structural studies (Breeze et al., 1991; Lynch and Kaiser, 1988). SecStr, though, suggests an alternative prediction for a β-conformation between residues 4–31. This overlapping prediction implies that almost the entire sequence of αCGRP has the distinctive features of a "chameleon" sequence (Kabsch and Sander, 1984) and therefore intrinsically exhibits the tendency to modify its conformation depending on environmental changes (Fig. S2).

Sequence alignments for comparison of important regions within each protein were performed using the Clustal Omega Multiple Sequence Alignment software (Sievers et al., 2011) and were illustrated using Jalview (Waterhouse et al., 2009) (Fig. S1).

2.2. Peptide synthesis

Four (4) αCGRP peptide-analogues were designed (Fig. 1A); two versions of the predicted 'aggregation-prone' region ^{6}TCVTHR^{11} (αCGRP1, αCGRP2) corresponding to the N-terminal of the mature αCGRP sequence, the ^{22}VVKNNFV^{28} (αCGRP3) segment corresponding to the central region of the mature αCGRP sequence and, finally, the ^{30}TNVGSKAF^{37} octapeptide (αCGRP4) corresponding to the C-terminal region. In the case of the ^{6}TCVTHR^{11} peptide, we designed the analogues ^{6}TAVTHR^{11} and ^{6}TmethCVTHR^{11} by replacing the cysteine 7 with alanine and a methylated cysteine, respectively, in order to prevent the formation of undesirable, intermolecular disulfide bonds between cysteines. We should mention that peptide-analogues αCGRP1, αCGRP2 are also 'aggregation-prone' peptides, according to computational prediction analyses (data not shown).

Peptide synthesis was performed by solid phase methodology and Fmoc/But chemistry, using 2-chlorotrityl chloride resin as a solid support (Barlos et al., 1989). Analytical HPLC was used in order to determine peptide purity (> 97%). The 37-aminoacid hormone αCGRP and the αCGRP4 peptide were prepared with amidated C-terminal ends and free N-terminals, since C-terminal amidation is a common and necessary feature for all members of the CGRP family (Poyner et al., 2002). Peptide-analogues αCGRP1, αCGRP2 and αCGRP3 have free N- and C-terminals.

2.3. Preparation of protein/peptide samples

Lyophilized aliquots of αCGRP hormone were re-suspended in distilled water (pH 5.5) at concentrations of 1 mg ml^{-1} and 10 mg ml^{-1}. Similarly, lyophilized peptide-analogues αCGRP1, αCGRP2, αCGRP3 and αCGRP4 were dissolved in distilled water (pH 5.75) at concentrations of up to 10 mg ml^{-1}. All solutions were found to produce gels after 1 to 7 days of incubation, depending on the sample.

2.4. X-ray diffraction

In order to produce oriented fibers a droplet (5 μl) of each peptide suspension at a concentration of 10 mg ml^{-1} was placed between two properly aligned siliconized glass rods (~2 mm apart). Each droplet was allowed to dry slowly at ambient temperature and humidity for approximately 30 min in order to form an oriented fiber suitable for X-ray diffraction. The X-ray diffraction patterns were collected, using a SuperNova-Agilent Technologies X-ray generator equipped with a 135-mm ATLAS CCD detector and a 4-circle kappa goniometer, at the Institute of Biology, Medicinal Chemistry and Biotechnology, at the National Hellenic Research Foundation, operated at 50 kV, 0.8 mA (CuK_α high intensity X-ray source, λ = 1.5418 Å). Specimen-to-film distance was specified at 52 mm, whereas exposure time was set to 400 s. Each X-ray pattern, was initially viewed using the CrysAlisPro software (CrysAlis^{PRO}, 2014) and consequently measured with the aid of the iMosFLM software (Leslie and Powell, 2007).

2.5. Negative staining

For negative staining, peptide solutions were independently applied to glow-discharged 400-mesh carbon-coated copper grids for approximately 90 s. The grids were stained with a drop (5 μl) of 2% (w/v) aqueous uranyl acetate for 60 s. Excess stain was removed by blotting with a filter paper and then the grids were air-dried. The fibril containing grids were examined with a Morgagni™ 268 transmission electron microscope, operated at 80 kV. Digital acquisitions were performed with an 11-Mpixel side-mounted Morada CCD camera (Soft Imaging System, Muenster, Germany).

2.6. Congo red staining

Fibril suspensions of the peptide solutions were applied to glass slides and were allowed to air-dry. The film formed by αCGRP was stained with a 10 mM Congo red solution in phosphate-buffered saline (pH 7.4) for approximately 1 h (Divry and Florkin, 1927). Excess staining was removed by several washes with 90% ethanol and left to dry at room temperature. The films produced by αCGRP1, αCGRP2, αCGRP3 and αCGRP4 were stained with a 1% Congo red solution in distilled water (pH 5.75) at room temperature for approximately 20 min, as indicated by the Romhanyi protocol and excess stain was removed through tap water washes (Bely and Makovitzky, 2006; Romhanyi, 1971). Subsequently, all the samples were observed under bright field illumination and between crossed polars, using a Leica $MZ_{7.5}$ polarizing stereomicroscope equipped with a JVC GC-X3E camera.

2.7. Attenuated total reflectance Fourier-transform infrared spectroscopy (ATR FT-IR) and post-run computations of the spectra

A drop (5 μl) of mature fibril suspensions of all five peptides were cast on a front-coated Au mirror and left to dry slowly at ambient conditions to form thin films. Infrared spectra were obtained from these films at a resolution of 4 cm^{-1}, utilizing an IR microscope (IRScope II by Bruker Optics) equipped with a Ge attenuated total reflectance (ATR) objective lens (20×) and attached to a Fourier-transform infrared (FTIR) spectrometer (Equinox 55, by Bruker Optics). Internal reflection spectroscopy has several advantages compared with the more common KBr dispersion technique (de Jongh et al., 1996). The choice of ATR was dictated by the need to exclude any possible spectroscopic and chemical interactions between the sample and the dispersing medium. Having a penetration depth ca. 1–2 μm (1000 cm^{-1}, Ge), ATR is free of saturation effects, which may be present in the transmission spectra of thicker samples. Moreover, the use of a microscope facilitates the acquisition of data from small samples. Ten 32-scan spectra were collected from each sample and averaged to improve the S/N ratio. The spectra are shown in the absorption mode after correction for the wavelength dependence of the penetration depth (pd ~ λ).

2.8. Computational modeling and structural analysis

Several experimental studies have attempted to accurately define the architecture of the polymorphic IAPP fibrillar structures (Bedrood et al., 2012; Luca et al., 2007; Wiltzius et al., 2008). The CreateFibril database stores a collection of computationally calculated stable polymorphic fibril models of HET-s, Aβ, and IAPP peptides, along with their structural energy landscapes (Smaoui et al., 2013). The monomeric amyloid form of IAPP, created by Wiltzius et al. was used as a starting template to build other polymorphic fibrils deposited in the CreateFibril database. The basic model, featuring five (5) copies of IAPP, is basically a fibrillar structure based on the crystal structures of NNFGAIL (PDB ID: 3DGJ) and SSTNVG (PDB ID: 3FTR) (Wiltzius et al., 2008).

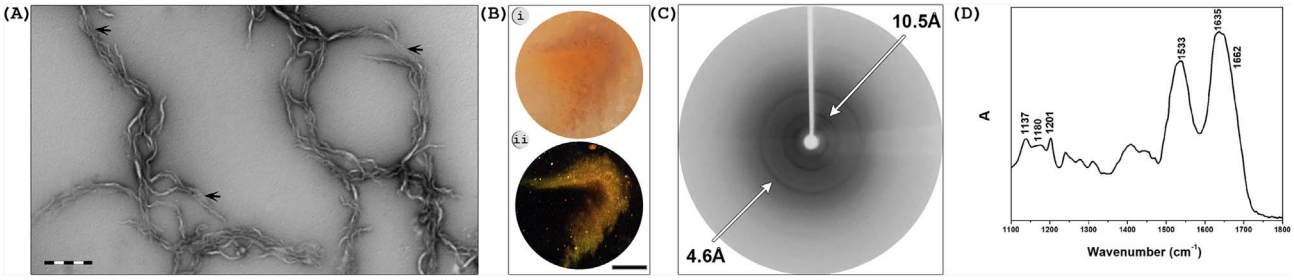

Fig. 2. Experimental results of full-length αCGRP. (A) Electron micrograph was taken after one week of incubation in distilled water. The sample was negatively stained with 2% uranyl acetate (See). Arrows show fibrils, approximately 10 nm in diameter (See Results). Bar 500 nm. (B) Photomicrographs of αCGRP peptide fibrils stained with Congo Red: bright field illumination (i), crossed polars (ii). The yellow-green birefringence, characteristic for amyloid fibrils, is clearly seen under crossed polars. Bar 500 μm. (C) X-ray diffraction pattern from oriented fibers of αCGRP peptide amyloid-like fibrils. The pattern illustrates the typical "cross-β" reflections. The appearance of rings, instead of oriented reflections at the meridian and at the equator, indicate a random packing of the constituent amyloid fibrils in the fiber. (D) ATR FT-IR spectra (1100–1800 cm^{-1}), obtained from suspensions of fibrils, produced from the αCGRP peptide, cast on a flat stainless-steel plate and left to air-dry slowly, at ambient conditions, to form hydrated, thin films (see also Table 1). (For interpretation of the references to color in this figure legend, the reader is referred to the web version of this article.)

Based on the high sequence homology between αCGRP and IAPP (approximately 43% sequence identity – Supplementary Fig. S1), a three-dimensional structure of αCGRP protofibrils was constructed utilizing Modeller9v12 (Eswar et al., 2006). The derived model consists of five copies of full-length αCGRP, organized in a single pentamer (Fig. S3A, henceforth called αCGRP-5mer). The subjected model was further edited with AmberTools 16 and the Amber-99sb-ildn force field, using the xLeap module to amidate the C-termini and the Sander module to perform steepest descent energy minimization (Lindorff-Larsen et al., 2010; Salomon-Ferrer et al., 2013). Fig. 1B illustrates an extracted misfolded monomer of αCGRP and records all distinct features of the mature protein. Higher order protofibril models, namely an αCGRP-stack and an αCGRP-polygon, were created using geometrical restraints as defined by the CreateFibril toolkit (Smaoui et al., 2013).

In addition to the full-length αCGRP protofibril models, starting configurations were also generated for the small αCGRP*1-4* oligopeptides. Initial, unstructured oligopeptides were built using xLeap (Salomon-Ferrer et al., 2013). The N- and C-termini were capped with neutral groups to remove unwanted charges. Each of the peptides was subjected to steepest descent energy minimization, followed by 1 ns of simulation in vacuum conditions with Sander, from which random configurations were selected. Four randomized copies of each peptide were scattered in a cubic box with an initial intermolecular distance of at least 1.0 nm between the peptides.

2.9. Molecular Dynamics

Molecular Dynamics simulations were performed in explicit aqueous solvent, using GROMACS v. 5.1.4 (Van Der Spoel et al., 2005), the AMBER ff99sb-ildn force field for proteins (Lindorff-Larsen et al., 2010) and the TIP3P water model (Jorgensen et al., 1983). The choice of force field was made with respect to the structural properties of the tested models; in general, the ff99sb-ildn variation of AMBER has been found to accurately reproduce evidence obtained from NMR and circular dichroism experiments on the secondary structure elements of oligopeptides and the folding of β-hairpin structures (Beauchamp et al., 2012; Koukos and Glykos, 2014), as well as the dynamics of IAPP and Aβ (Hoffmann et al., 2015; Somavarapu and Kepp, 2015).

In order to generate starting conformations, each protein system was embedded in a cubic solvent box with a distance of at least 1.2 nm between the box boundaries and protein coordinates. The systems were solvated using a 0.15 M NaCl concentration as well as neutralizing counter-ions, mimicking physiological pH conditions. Each system was subjected to extensive steepest descent energy minimization and was subsequently equilibrated with position restraints on protein atoms in two stages, namely, 500 ps of equilibration in the canonical (NVT) ensemble and 1 ns of equilibration in the isothermal-isobaric (NPT) ensemble. Another NPT equilibration followed for 1 ns without any restraints. Finally, each system was simulated in the NPT ensemble for production simulations. Full-length αCGRP oligomeric assemblies were simulated for 200 ns (Fig. S3), with each production simulation replicated in duplicate for validation. A description of the simulation systems is given in Simulation Table S1. Details on the simulation protocol are given in the Supplementary Material, available online.

3. Results and discussion

Amyloidogenesis is a generic phenomenon of polypeptide chains, since under appropriate conditions a great number of proteins, not strictly related with diseases, have been proven to convert to the amyloid state (Dobson, 1999). Although, recent studies revealed that a common amyloid architecture may signify conserved protein misfolding pathways *in vivo* (Annamalai et al., 2017), the *in vitro* elucidation of the polymerization has unraveled distinct fibrillation properties and a diversity of the aggregation capacity, among different protein systems (Fandrich et al., 2009; Tycko, 2015). The goal of this study was to examine the aggregation potency of αCGRP, an important member of the CGRP family, utilizing a combined approach of established biophysical experimental techniques, together with computational simulations.

3.1. Full length αCGRP fulfills all amyloid criteria

αCGRP amyloidogenicity was initially investigated by negative staining transmission electron microscopy. The αCGRP electron micrograph (Fig. 2A) demonstrates that the 37-amino acid hormone self-assembles into explicit fibrillar structures. These fibrils were formed after one week of incubation in distilled water at pH 5.5. The thinnest fibrils observed had a diameter of approximately 10 nm (Fig. 2A – arrows) and seem to have the tendency to wound around each other, giving rise to helical twisted fibrillar ultrastructures of several diameters. As shown in Fig. 2A, these ultrastructures interact laterally to form thick bundles and, subsequently, create periodic 'ring-like' arrangements, distributed evenly on the surface of the grid. Actually, the overall shape of amyloid structures, produced *in vitro*, depends on the conditions in which the polymerization occurs (Wetzel et al., 2007), since amyloids exhibit a unique plasticity, resulting to a wide range of amyloid species (microcrystals (Tsiolaki et al., 2015), spherulites (Krebs et al., 2009), triangles and squares (de Messieres et al., 2016)). This characteristic morphological variability of amyloid fibrils has also been observed among the already known amyloidogenic members of the CGRP family (Bauer et al., 1995; Goldsbury et al., 1997). Interestingly, alternative ways of lateral association of IAPP protofilaments emerge as a result of significant pH modifications (Jaikaran et al., 2001).

Congo red, an amyloid specific dye, binds to mature fibrils derived from αCGRP peptide, as shown in the bright field panel in Fig. 2B-i and

Table 1
Bands observed in the ATR FT-IR spectra obtained from thin-films, containing suspensions of fibrils, produced by the αCGRP peptide and αCGRP1-4 peptide-analogues, respectively and their tentative assignments.

Bands (cm^{-1})					Assignments
αCGRP	αCGRP1	αCGRP2	αCGRP3	αCGRP4	
1662	1666	1666	1670	1662	TFA
1635	1634	1631	1625	1635	β-sheet (Amide I)
1533	1529	1531	1537	1527	β-sheet (Amide II)
1201	1201	1199	1201	1199	TFA
1180	1182	1182	1184	1182	TFA
1137	1133	1132	1132	1134	TFA

*TFA (trifluoracetic acid), a component of peptide synthesis.

subsequently exhibits a diagnostic yellow-green birefringence when placed under crossed polars of a polarizing microscope (Fig. 2B-ii).

Since cross-β architecture is the universal energetic minimum for prone-to-aggregate proteins (Dobson, 2001), suitably prepared fibers, containing αCGRP amyloid fibrils, (see Section 2) were used to examine the structural organization of the polymerized αCGRP peptide. Apparently, the derived X-ray diffraction pattern is indicative of a "cross-β" conformation, displaying a 4.6 Å reflection on the meridian and a 10.5 Å reflection on the equator. Namely, these reflections correspond to the distance between repetitive hydrogen-bonding β-strands that extend along the length of the fibril and to the packing between adjacent β-sheets, respectively (Fig. 2C).

Spectral acquisition by ATR FT-IR spectroscopy has been also shown to render rich information about the secondary structure of αCGRP amyloid fibrils. The ATR FT-IR spectrum (Fig. 2D) shows a prominent band at 1635 cm^{-1} in the amide I region, which is clearly due to β-sheet conformation (Haris and Chapman, 1995; Jackson and Mantsch, 1995; Krimm and Bandekar, 1986; Surewicz et al., 1993; Valenti et al., 2011). Table 1 presents all measured bands and their assignments. Thus, the spectrum presented in Fig. 2D supports the presence of β-sheets in the structure of the polymerized αCGRP peptide, apparently in agreement with the existence of the β-sheet structure suggested by X-ray diffraction (Fig. 2C) and Congo red binding data (Fig. 2B).

The self-polymerization properties of αCGRP, reported here, strengthen previous intriguing analyses. Abe et al. revealed back in 1992 that CGRP is a component of amyloid of endocrine origin. Surprisingly, these immunoreactivity assays reported the presence of CGRP, deposited as stromal amyloids in a human atypical carcinoid tumor (Abe et al., 1992). Hubbard et al., ten years after Abe's case study, unraveled the unique finding of CGRP by using polyclonal antihuman amyloid component antibodies, for proteins of interest in unhealthy primates. The above immunohistochemical studies showed the presence and the crucial implication of both IAPP and CGRP in baboons with pancreatic islet amyloidosis (Hubbard et al., 2002). However, the crucial role of misfolded IAPP in the development of T2D in human was already established at that time (Westermark et al., 1986). The high sequence similarity between IAPP and CGRP (Fig. S1), though, raises the question whether these two peptide hormones use their shared epitopes to attract cross-reacting components of each immunoassay.

A subject of intense debate is that besides the major constituent protein recorded, a "cocktail" of deposited misfolded proteins is usually implicated in the pathogenesis of several disorders (especially in systemic amyloidoses), (Bergstrom et al., 2004; de Sousa et al., 2000; Levy et al., 2001). In this respect, another interesting finding emerged from a mass spectrometry approach, when Morris et al. isolated CGRP from the thyroid of patients with MTC. Researchers, apart from the calcitonin implication, suspected the involvement of CGRP in such an amyloidosis, and thus, they suggested that it is possibly responsible for some of the symptoms in the MTC (Morris et al., 1984). Clear identification of the primary structure of a misfolded protein, though, requires isolation of the fibrillar species and molecular determination of its sequence, a process that is often exhausting and unsuccessful (Rocken and Sletten, 2003). Nevertheless, it is worth mentioning that, abnormal self-aggregation may trigger irregular interactions between proteins within the crowded molecular environment of a tissue, leading to a cascade of massive protein deposition, as reported in *in vitro* assays (Guo et al., 2006; Morales et al., 2010; Tsigelny et al., 2008; Ulbrich et al., 2014; Westermark and Westermark, 2008; Yan et al., 2007) or in transgenic animal models (Gotz et al., 2001; Morales et al., 2010).

3.2. Aggregation assays of αCGRP peptide-analogues

Various studies have indicated that short fragments with high aggregation propensity, hidden in the primary sequence, may stimulate the aggregation tendency of a protein (Frousios et al., 2009; Lopez de la Paz and Serrano, 2004). αCGRP, IAPP and calcitonin show high degree of homology, implying that all three peptide hormones may share common 'aggregation-prone' regions (Fig. S1). Towards this end, we designed and synthesized four αCGRP peptide-analogues, representing crucial segments of IAPP and calcitonin amyloidogenicity. Firstly, the αCGRP N-terminal hexapeptide ^{6}TCVTHR^{11} (αCGRP1 & αCGRP2) was designed, based on our previous studies on an homologous calcitonin peptide-analogue (^{6}TCMLGT^{11}) (Iconomidou et al., 2013). Secondly, high sequence similarity between the αCGRP and IAPP (Fig. S1) and evidence at experimental level linking the central region and the C-terminal region of IAPP with amyloidogenicity (Jaikaran and Clark, 2001; Westermark et al., 1990), led us to also design a central region peptide-analogue (αCGRP3 – ^{22}VVKNNF^{27}) and a C-terminal peptide-analogue (αCGRP4 – ^{30}TNVGSKAF^{37}) (Fig. S1). Electron microscopy, X-ray fiber diffraction, Fourier transform infrared spectroscopy and Congo Red staining were used simultaneously to examine the amyloidogenic properties of all designed αCGRP peptide-analogues. Exploring segments associated with amyloidogenicity is pivotal for a clear understanding of segments, governing αCGRP fibril formation.

Electron microscopy studies demonstrated that peptides αCGRP1, αCGRP2 and αCGRP4 self-assemble into typical amyloid fibrils (Fig. 3A-i, 3B-i & 3D-i), with the exception of αCGRP3, which apparently forms amorphous aggregates (Fig. 3C-i). Interestingly, peptides αCGRP1 and αCGRP2, varying in only one amino acid residue, are shown to form distinct fibril populations (Wetzel et al., 2007). On the other hand, αCGRP3 amorphous aggregates highlight one impressive difference between the amyloidogenic profile of a CGRP and IAPP, two highly similar peptide hormones (Fig. S1).

X-ray diffraction data and spectral acquisition by ATR FT-IR spectroscopy experiments reveal that all four (4) peptide-analogues have overall well ordered β-structures (Figs. 3 and 4). Table 1 summarizes all ATR FT-IR measured bands and their tentative assignments. However, ATR FT-IR spectroscopy does not provide a distinctive spectral signature for the cross-β architecture, found to constitute the amyloid core. It is noteworthy that, despite its decreased amyloidogenicity, αCGRP3 structural data, derived from X-ray fiber diffraction and ATR FT-IR spectroscopy, reveal an unexpected β-sheet architecture. Support for this finding comes from past and recent studies, suggesting also a β structure for amorphous aggregates (Huang et al., 2000; Shivu et al., 2013). In the case of αCGRP4, X-ray diffraction revealed an oriented diffraction pattern, exhibiting an intense reflection at 4.7 Å and a weak and diffuse reflection at 11 Å. This indicates that the packing between β-sheets is less uniform in comparison with the β-strand packing in the fiber of αCGRP4, a phenomenon that has also been observed in many other amyloidogenic samples (Ivanova et al., 2009; Mossuto et al., 2010).

The amyloid specific Congo red dye has been shown to selectively bind only on αCGRP1, αCGRP2 and αCGRP4 peptide-analogues, exhibiting yellow/green birefringence, when viewed under crossed polars of a polarizing microscope (Fig. 3A-iii, 3B-iii & 3D-iii). αCGRP3 amorphous aggregates were not able to produce the characteristic birefringence and this finding, in turn, verifies that Congo red has high

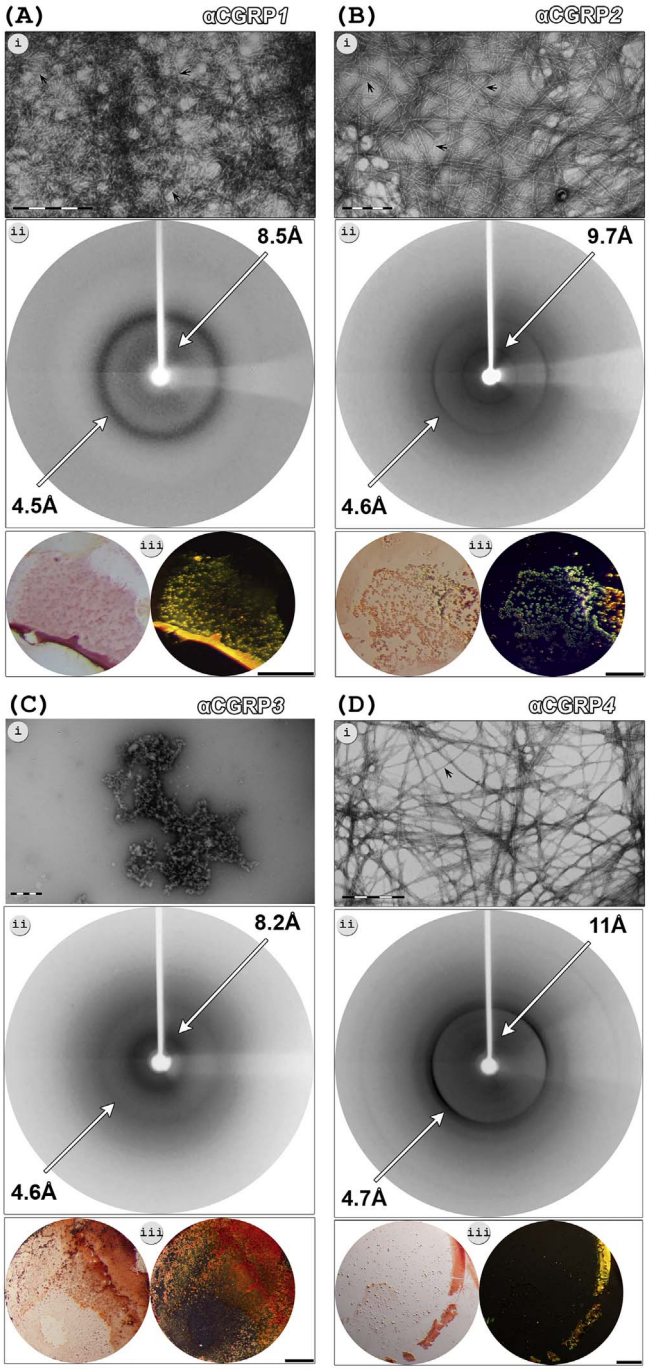

Fig. 3. Amyloidogenic properties of the αCGRP1, αCGRP2, αCGRP3 and αCGRP4 "aggregation-prone" peptides (A–D). Peptide-analogues αCGRP1 (A-i), αCGRP2 (B-i) and αCGRP4 (D-i) self-assemble forming straight and unbranched amyloid-like fibrils, approximately 100 Å in diameter, with the exception of αCGRP3 (C-i), which forms amorphous aggregates (Scale bars 400 nm). An apparent apple-green birefringence characteristic for amyloid deposits, produced only by αCGRP1 (A-ii), αCGRP2 (B-ii) and αCGRP4 (D-ii) fibril-containing gels, is clearly seen under crossed polars (Scale bars 500 μm). Impressively, all X-ray fiber diffraction patterns (A-iii, B-iii, C-iii, D-iii) exhibit the typical "cross-β" architecture reflections, with a 4.5–4.7 Å repeat corresponding to the distance of hydrogen bonded-strands and the 8.2, 8.5, 9.7 and 11 Å reflections representing the distance between the packed–sheets. In well oriented fibril samples the reflections appear as arcs and have distinct positions, whereas other reflections may appear as rings due to rather poor alignment of the constituent fibrils. (For interpretation of the references to color in this figure legend, the reader is referred to the web version of this article.)

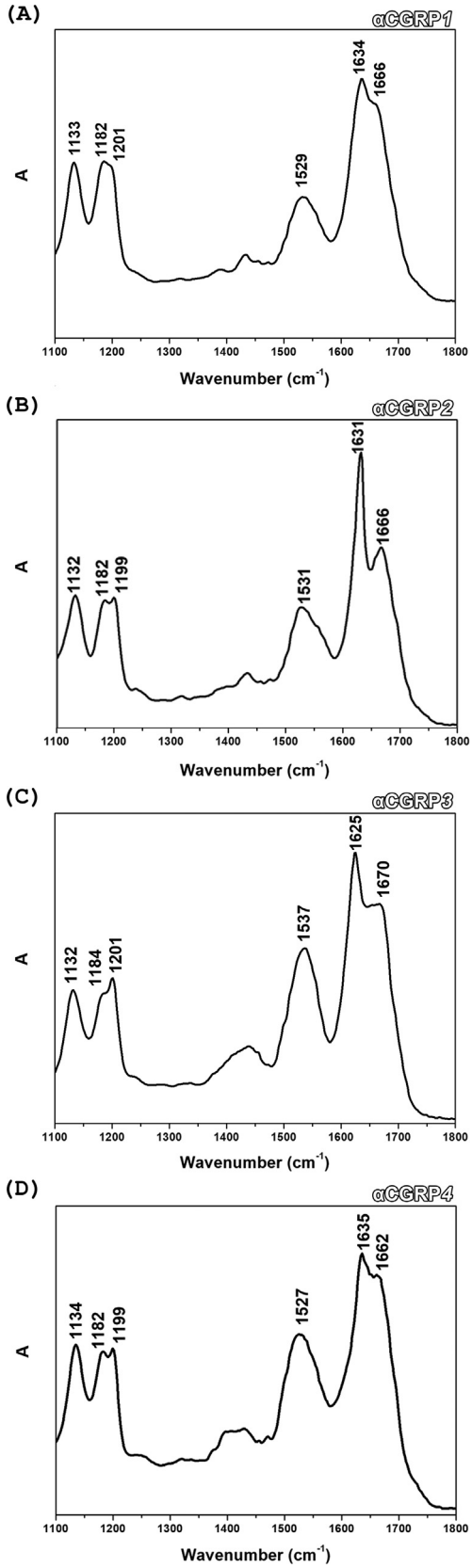

Fig. 4. ATR FT-IR spectra (1100–1800 cm^{-1}) produced from thin hydrated films containing aggregates derived by the self-polymerizing (A) αCGRP1, (B) αCGRP2 (C) αCGRP3 (D) αCGRP4. Fibrils derived by each peptide possess a β-sheet secondary structure, as it is clearly evident by the presence of strong amide I and II bands (see also Table 1).

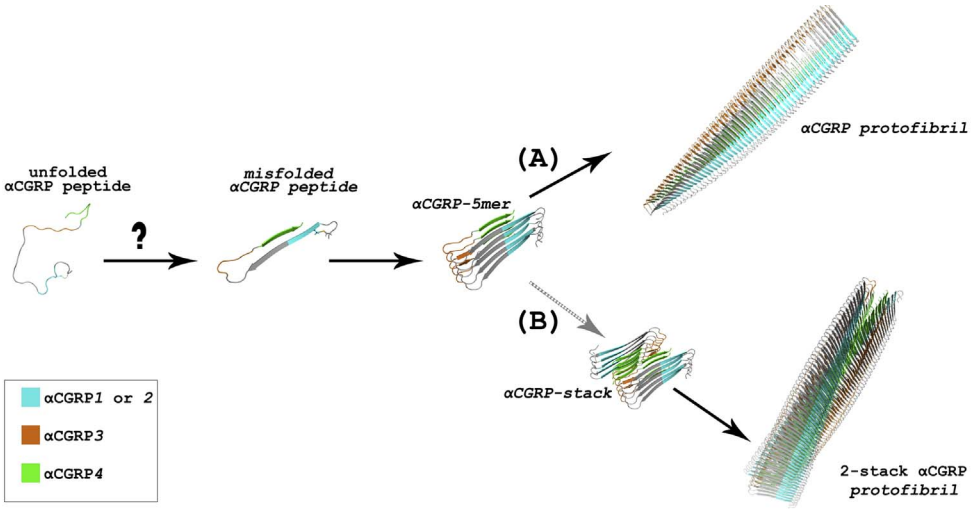

Fig. 5. The step-to-step polymerization mechanism of αCGRP, based on MD simulations. Under denaturing conditions, αCGRP amyloid fibril formation is accompanied by a conformational change from random coil to β-sheet. Unfolded αCGRP may misfold by adopting a U-shaped topology (β-strand – loop – β-strand). Two alternative polymerization pathways (A & B) are suggested. U-shaped monomers organized into pentamers and stabilized by intermolecular backbone-backbone hydrogen bonds (αCGRP-5mer) may elongate by the continual rigid placement of monomers on both sides and form a single αCGRP protofibril (A). A higher order oligomeric conformation may arise, if an intermediate oligomeric state is formed (αCGRP-stack) prior to the protofibril formation. The twofold symmetric αCGRP-stack oligomer is the second more stable shape, allowing to suggest an alternative assembly mechanism, namely, the creation of a 2-stack αCGRP-protofibril (B). Polymorphic protofibrils of αCGRP were produced with the aid of CreateFibril routines (Smaoui et al., 2013), whereas intermediate states were constructed and evaluated by MD simulations in explicit aqueous solvent (See). αCGRP1-4 peptide-analogues are shown in cyan (1 and 2), orange (3) and green (4), respectively. A color index is provided. (For interpretation of the references to color in this figure legend, the reader is referred to the web version of this article.)

affinity only for ordered fibrillar structures (Frid et al., 2007) (Fig. 3C-iii).

3.3. Insights of αCGRP fibrillation from Molecular Dynamics simulations

Molecular Dynamics (MD) simulations were performed in order to correlate our experimental observations with a specific mechanism of αCGRP polymerization. αCGRP modeling was based on its amyloidogenic properties (See Figs. 2–4), and its sequence similarity to IAPP (See Fig. S1 & Section 2). Three (3) forms of αCGRP oligomers were created, in agreement with solid-state NMR fibrillar architectures of $A\beta_{1-40}$ (Paravastu et al., 2008) or IAPP (Luca et al., 2007) available in CreateFibril database (Smaoui et al., 2013); a single pentamer (Fig. S3A, henceforth called αCGRP-5mer), a decamer stack consisting of two αCGRP-5mers (Fig. S3B, henceforth termed αCGRP-stack) and a pentadecamer consisting of three αCGRP-5mers in a polygon organization (Fig. S3C, henceforth termed αCGRP-polygon). The stability and dynamic behavior of αCGRP-5mer, αCGRP-stack and αCGRP-polygon were further evaluated through MD simulations, conducted in explicit aqueous solvent (Fig. S3). Table S1 gathers details of each simulation system, described hereupon.

The αCGRP-5mer retains its parallel β-strands and U-shaped topology throughout the simulations, with the monomers adopting a twist angle of ~ 4-6° between adjacent β-strands in the protofibril core (Fig. S3A). A time-dependent RMSD measurement from the starting conformations-of the simulations (aver. RMSD ~ 6.5 Å for the final 40 ns) and a per-residue analysis of fluctuations, as reflected by RMSF calculations, are shown in Fig. S4. The most stable regions of the model include the 6–15 and 25–33 segments of each monomer, corresponding to regions forming β-strands. Impressively, αCGRP1 and αCGRP2 peptide-analogues, corresponding to region 6–15, and αCGRP4, corresponding to region 30–37, were experimentally found to form amyloid-like fibrils (Fig. 3A, B & D). Significant fluctuations, observed for the 16–27 region particularly for the monomers at the two ends of the pentamer, can be attributed to the repulsive interactions between two positively charged residues (Arg-18 and Lys-24), located in the loop region. This loss of packing, though, is in agreement with experimental evidence, as the αCGRP3 peptide-analogue, corresponding to this particular segment, was shown to form amorphous aggregates (Fig. 3C).

The extent of movement differs between the αCGRP-stack and the αCGRP-polygon system. The αCGRP-stack dissociates only partially, since the β-sheet segments increase the distance of the two pentamers. Impressively, despite the movements of the adjacent pentameric units, their overall U-bend structure remains stable, displaying many of the characteristics observed in the αCGRP-5mer simulations (Fig. S3B). The αCGRP-polygon, on the other hand, showed rapid disassembly of the original complex (Fig. S3C). A possible reason for this could be the presence of several solvent-exposed Lys residues in αCGRP, resulting in an overall positive electrostatic potential of the model surface. Overall, the αCGRP-stack and the αCGRP-polygon tests indicate that the tested packing schemes are thermodynamically unfavorable, although none of the tested simulations showed complete dissociation (Fig. S3B and C).

Evidence indicative of the native αCGRP three-dimensional conformation, has emerged from structural studies in different solutions. NMR spectra reported that αCGRP in aqueous solutions lacks any secondary structure content (Breeze et al., 1991), whereas at the same time CD studies revealed the solvent-dependent tendency of the αCGRP peptide to adopt an α-helical conformation (Lynch and Kaiser, 1988). However, sequence analyses of αCGRP presented here reveals distinctive "chameleon" properties (Kabsch and Sander, 1984) for the αCGRP polypeptide chain (Fig. S2), bearing a notable amyloidogenic profile.

Natively disordered proteins are particularly susceptible to aggregation (Fraga et al., 2014). Supposing that αCGRP is one of the many examples of natively disordered proteins able to convert into the amyloid state (Nelson and Eisenberg, 2006), we built a step-to-step scheme of its potential self-aggregation, based on our consistent experimental and computational results. Destabilizing conditions may facilitate amyloidogenesis by converting natively unfolded αCGRP peptide into a misfolded αCGRP peptide, exposing its aggregation-prone surfaces (peptides αCGRP1 or 2 and αCGRP4) to neighboring molecules. The proposed mechanism of αCGRP polymerization may involve two alternative routes of self-aggregation. Misfolded monomers organized into pentamers (αCGRP-5mer) may elongate by the continual stacking of monomers on both sides and form a single αCGRP protofibril. Alternatively, an intermediate oligomeric state can be formed (αCGRP-stack) prior to the protofibril assembly, suggesting a different, albeit less favorable, assembly mechanism, namely, the creation of a 2-stack αCGRP-protofibril (Fig. 5). Impressively, all fragments, corresponding to αCGRP1-4 peptide-analogues, are found to contribute to the interface interactions between separate αCGRP protofibrils, meaning that they tend to interact by tracking themselves into adjacent protofibrils (Fig. 5, cyan/orange/green).

In addition to full-length αCGRP, equilibrium MD simulations were conducted to study the self-assembly capabilities of the αCGRP1-4 peptide-analogues, outside the framework of the proposed full-length

model (Fig. S5). For each case, a solvent box containing four copies of each peptide with random conformations was simulated in the microsecond scale (See Section 2). An inspection of the simulation results shows that in all cases the peptides diffused freely in their simulation box, leading to multiple spontaneous association and dissociation events. This finding is in agreement with results from MD simulations of the early oligomerization events for the amyloidogenic GNNQQNY peptide, which showed that multiple association and dissociation events can occur in the nanosecond to microsecond timescale (Zhang et al., 2007).

Of the four systems sampled, the αCGRP1 (Fig. S5A) and αCGRP2 (Fig. S5B) simulations displayed the most profound association properties and eventually formed peptide aggregates that were retained until the end of their 1 μs simulations. Similar aggregates were also observed for the αCGRP4 system, corresponding to the C-terminal, amyloidogenic 30–37 region of αCGRP, although these aggregates eventually dissociated (Fig. S5D). The lifetime of formed aggregates throughout these simulations is relatively long, ranging from 100 to 200 ns before dissociation. In contrast, all associated aggregates observed in the αCGRP3 simulations were short-lived, dissociating within 10–20 ns from their formation (Fig. S5C). Although, as already stated, these observations cannot provide any information on aggregation kinetics, they do indicate that, overall, the αCGRP3 segment displays limited aggregation capabilities compared to αCRP1, αCGRP2 and αCGRP4, in agreement with the experimental results (Fig. 3). As far as the secondary structure is concerned, the complexes produced by the αCGRP1 and αCGRP2 systems and, to a lesser extent, the αCGRP4 system, adopted β-structure characteristics reminiscent of aggregates previously observed in GNNQQNY simulations (Zhang et al., 2007). On the other hand, the complexes observed in the αCGRP3 simulations were amorphous, with some of the peptides even transiently adopting helix-like characteristics (data not shown).

Impressively, the above observations are in agreement with the simulation results of full-length αCGRP, showing the strong β-structure characteristics of the 6–11 segment, corresponding to αCGRP1-2, the partially ordered nature of the 30–37 segment corresponding the αCGRP4 and the mainly coil/amorphous nature of the 22–28 region corresponding to αCGRP3. The spatial implication of αCGRP1-4 peptide-analogues in each oligomer is highlighted in Fig. 5 (See also Fig. 5 legend).

4. Conclusions

αCGRP has become a subject of intensive investigation due to its variety of biological effects in the CNS or in peripheral tissues. The apparent existence of αCGRP in well-studied amyloidoses, such as the T2D and MTC, lead us to examine its unexplored amyloidogenic profile and its relative role, utilizing a combination of experimental and computational tests. Overall, experimental assays detected characteristic amyloidogenic properties for the full-length αCGRP peptide hormone, similarly to calcitonin and IAPP, whereas analogous experiments tracked the hidden amyloidogenic characteristics of N- and C- terminal regions of the αCGRP. MD simulations, on the other hand, displayed that the pentameric U-bend fold is a favorable assembly for the full-length αCGRP, although modifications may be needed in order to achieve an optimized structure. Although it is possible for the fibrils in tissues to be functionally different from the fibrils produced *in vitro*, our results bring to light a novel and intriguing feature of αCGRP which may answer crucial questions to the succession of events, occurring during the pathogenesis of the above disorders.

Conflict of interest

The authors declare no conflicts of interest.

Acknowledgments

We thank the Institute of Biology, Medicinal Chemistry and Biotechnology at National Hellenic Research Foundation for access to the X-ray diffraction facility. We acknowledge the help of Dr. Evangelia Chrysina with the X-ray diffraction experiments. The help of Dr. George Baltatzis and Prof. Efstratios Patsouris and the use of the Morgagni Microscope at the 1st Department of Pathology, Medical School, National and Kapodistrian University of Athens are also gratefully acknowledged. Finally, we would like to thank the handling editor and the anonymous reviewers of this manuscript for their useful and constructive criticism.**Funding**

This work was supported by computational time granted from the Greek Research & Technology Network (GRNET) in the National HPC facility – ARIS under project ID “PR003002-AmyloidDiabetes”.

Appendix A. Supplementary data

Available PDB-format coordinate sets associated with MD simulations. Supplementary data associated with this article can be found, in the online version, at http://dx.doi.org/10.1016/j.jsb.2018.02.008.

References

Abe, Y., Utsunomiya, H., Tsutsumi, Y., 1992. Atypical carcinoid tumor of the lung with amyloid stroma. Acta Pathol. Jpn. 42, 286–292.
Amara, S.G., Jonas, V., Rosenfeld, M.G., Ong, E.S., Evans, R.M., 1982. Alternative RNA processing in calcitonin gene expression generates mRNAs encoding different polypeptide products. Nature 298, 240–244.
Amara, S.G., Arriza, J.L., Leff, S.E., Swanson, L.W., Evans, R.M., Rosenfeld, M.G., 1985. Expression in brain of a messenger RNA encoding a novel neuropeptide homologous to calcitonin gene-related peptide. Science 229, 1094–1097.
Andreotti, G., Mendez, B.L., Amodeo, P., Morelli, M.A., Nakamuta, H., Motta, A., 2006. Structural determinants of salmon calcitonin bioactivity: the role of the Leu-based amphipathic alpha-helix. J. Biol. Chem. 281, 24193–24203.
Annamalai, K., Liberta, F., Vielberg, M.T., Close, W., Lilie, H., Guhrs, K.H., Schierhorn, A., Koehler, R., Schmidt, A., Haupt, C., Hegenbart, U., Schonland, S., Schmidt, M., Groll, M., Fandrich, M., 2017. Common fibril structures imply systemically conserved protein misfolding pathways in vivo. Angew. Chem. Int. Ed. Engl. 56, 7510–7514.
Ashkenazi, Y., Hersko, C., Gafni, J., Sohar, E., Heller, H., 1967. Chemical aspects of amyloid-Congo red binding. Isr. J. Med. Sci. 3, 572–574.
Barlos, K., Gatos, D., Kallitsis, J., Papaphotiu, G., Sotiriu, P., Wenqing, Y., Schäfer, W., 1989. Darstellung geschützter peptid-fragmente unter einsatz substituierter triphenylmethyl-harze. Tetrahed. Lett. 30, 3943–3946.
Bauer, H.H., Aebi, U., Haner, M., Hermann, R., Muller, M., Merkle, H.P., 1995. Architecture and polymorphism of fibrillar supramolecular assemblies produced by in vitro aggregation of human calcitonin. J. Struct. Biol. 115, 1–15.
Beauchamp, K.A., Lin, Y.S., Das, R., Pande, V.S., 2012. Are protein force fields getting better? A systematic benchmark on 524 diverse NMR measurements. J. Chem. Theory. Comput. 8, 1409–1414.
Bedrood, S., Li, Y., Isas, J.M., Hegde, B.G., Baxa, U., Haworth, I.S., Langen, R., 2012. Fibril structure of human islet amyloid polypeptide. J. Biol. Chem. 287, 5235–5241.
Bely, M., Makovitzky, J., 2006. Sensitivity and specificity of Congo red staining according to Romhanyi. Comparison with Puchtler's or Bennhold's methods. Acta Histochem. 108, 175–180.
Bergstrom, J., Murphy, C.L., Weiss, D.T., Solomon, A., Sletten, K., Hellman, U., Westermark, P., 2004. Two different types of amyloid deposits–apolipoprotein A-IV and transthyretin–in a patient with systemic amyloidosis. Lab. Invest. 84, 981–988.
Brain, S.D., Grant, A.D., 2004. Vascular actions of calcitonin gene-related peptide and adrenomedullin. Physiol. Rev. 84, 903–934.
Breeze, A.L., Harvey, T.S., Bazzo, R., Campbell, I.D., 1991. Solution structure of human calcitonin gene-related peptide by 1H NMR and distance geometry with restrained molecular dynamics. Biochemistry 30, 575–582.
Chiti, F., Dobson, C.M., 2006. Protein misfolding, functional amyloid, and human disease. Annu. Rev. Biochem. 75, 333–366.
Conner, A.C., Hay, D.L., Howitt, S.G., Kilk, K., Langel, U., Wheatley, M., Smith, D.M., Poyner, D.R., 2002. Interaction of calcitonin-gene-related peptide with its receptors. Biochem. Soc. Trans. 30, 451–455.
Copp, D.H., Cheney, B., 1962. Calcitonin-a hormone from the parathyroid which lowers the calcium-level of the blood. Nature 193, 381–382.
CrysAlisPRO, 2014. Agilent Technologies, pp. Software system, Version 1.171.37.31 ed. Agilent Technologies UK Ltd, Oxford, UK.
de Jongh, H.H., Goormaghtigh, E., Ruysschaert, J.M., 1996. The different molar absorptivities of the secondary structure types in the amide I region: an attenuated total reflection infrared study on globular proteins. Anal. Biochem. 242, 95–103.
de Messieres, M., Ng, A., Duarte, C.J., Remaley, A.T., Lee, J.C., 2016. Single-particle tracking of human lipoproteins. Anal. Chem. 88, 596–599.

de Sousa, M.M., Vital, C., Ostler, D., Fernandes, R., Pouget-Abadie, J., Carles, D., Saraiva, M.J., 2000. Apolipoprotein AI and transthyretin as components of amyloid fibrils in a kindred with apoAI Leu178His amyloidosis. Am. J. Pathol. 156, 1911–1917.
Divry, D., Florkin, M., 1927. Sur les proprietes optiques de l'amyloide. Comptes Rendus de la Societe de Biologie 97, 1808–1810.
Dobson, C.M., 1999. Protein misfolding, evolution and disease. Trends Biochem. Sci. 24, 329–332.
Dobson, C.M., 2001. The structural basis of protein folding and its links with human disease. Philos. Trans. R. Soc. Lond. B. Biol. Sci. 356, 133–145.
Doods, H., Hallermayer, G., Wu, D., Entzeroth, M., Rudolf, K., Engel, W., Eberlein, W., 2000. Pharmacological profile of BIBN4096BS, the first selective small molecule CGRP antagonist. Br. J. Pharmacol. 129, 420–423.
Eichner, T., Radford, S.E., 2011. A diversity of assembly mechanisms of a generic amyloid fold. Mol. Cell. 43, 8–18.
Eswar, N., Webb, B., Marti-Renom, M.A., Madhusudhan, M.S., Eramian, D., Shen, M.Y., Pieper, U., Sali, A., 2006. Comparative protein structure modeling using Modeller. Curr. Protoc. Bioinform Chapter 5, Unit 5 6.
Fandrich, M., Meinhardt, J., Grigorieff, N., 2009. Structural polymorphism of Alzheimer Abeta and other amyloid fibrils. Prion 3, 89–93.
Fox, A., Snollaerts, T., Errecart Casanova, C., Calciano, A., Nogaj, L.A., Moffet, D.A., 2010. Selection for nonamyloidogenic mutants of islet amyloid polypeptide (IAPP) identifies an extended region for amyloidogenicity. Biochemistry 49, 7783–7789.
Fraga, H., Grana-Montes, R., Illa, R., Covaleda, G., Ventura, S., 2014. Association between foldability and aggregation propensity in small disulfide-rich proteins. Antioxid. Redox Signal. 21, 368–383.
Frid, P., Anisimov, S.V., Popovic, N., 2007. Congo red and protein aggregation in neurodegenerative diseases. Brain Res. Rev. 53, 135–160.
Frousios, K.K., Iconomidou, V.A., Karletidi, C.M., Hamodrakas, S.J., 2009. Amyloidogenic determinants are usually not buried. BMC Struct. Biol. 9, 44.
Goldsbury, C.S., Cooper, G.J., Goldie, K.N., Muller, S.A., Saafi, E.L., Gruijters, W.T., Misur, M.P., Engel, A., Aebi, U., Kistler, J., 1997. Polymorphic fibrillar assembly of human amylin. J. Struct. Biol. 119, 17–27.
Gotz, J., Chen, F., van Dorpe, J., Nitsch, R.M., 2001. Formation of neurofibrillary tangles in P301l tau transgenic mice induced by Abeta 42 fibrils. Science 293, 1491–1495.
Guo, J.P., Arai, T., Miklossy, J., McGeer, P.L., 2006. Abeta and tau form soluble complexes that may promote self aggregation of both into the insoluble forms observed in Alzheimer's disease. Proc. Natl. Acad. Sci. U.S.A. 103, 1953–1958.
Hamodrakas, S.J., 1988. A protein secondary structure prediction scheme for the IBM PC and compatibles. Comput. Appl. Biosci. 4, 473–477.
Haris, P.I., Chapman, D., 1995. The conformational analysis of peptides using Fourier transform IR spectroscopy. Biopolymers 37, 251–263.
Hazard, J.B., Hawk, W.A., Crile Jr., G., 1959. Medullary (solid) carcinoma of the thyroid; a clinicopathologic entity. J. Clin. Endocrinol. Metab. 19, 152–161.
Hoffmann, K.Q., McGovern, M., Chiu, C.C., de Pablo, J.J., 2015. Secondary structure of rat and human amylin across force fields. PloS One 10, e0134091.
Huang, T.H., Yang, D.S., Fraser, P.E., Chakrabartty, A., 2000. Alternate aggregation pathways of the Alzheimer beta-amyloid peptide. An in vitro model of preamyloid. J. Biol. Chem. 275, 36436–36440.
Hubbard, G.B., Steele, K.E., Davis 3rd, K.J., Leland, M.M., 2002. Spontaneous pancreatic islet amyloidosis in 40 baboons. J. Med. Primatol. 31, 84–90.
Iconomidou, V.A., Leontis, A., Hoenger, A., Hamodrakas, S.J., 2013. Identification of a novel 'aggregation-prone'/'amyloidogenic determinant' peptide in the sequence of the highly amyloidogenic human calcitonin. FEBS Lett. 587, 569–574.
Ivanova, M.I., Sievers, S.A., Sawaya, M.R., Wall, J.S., Eisenberg, D., 2009. Molecular basis for insulin fibril assembly. Proc. Natl. Acad. Sci. U.S.A. 106, 18990–18995.
Jackson, M., Mantsch, H.H., 1995. The use and misuse of FTIR spectroscopy in the determination of protein structure. Crit. Rev. Biochem. Mol. Biol. 30, 95–120.
Jaikaran, E.T., Clark, A., 2001. Islet amyloid and type 2 diabetes: from molecular misfolding to islet pathophysiology. Biochim. Biophys. Acta 1537, 179–203.
Jaikaran, E.T., Higham, C.E., Serpell, L.C., Zurdo, J., Gross, M., Clark, A., Fraser, P.E., 2001. Identification of a novel human islet amyloid polypeptide beta-sheet domain and factors influencing fibrillogenesis. J. Mol. Biol. 308, 515–525.
Jorgensen, W.L., Chandrasekhar, J., Madura, J.D., Impey, R.W., Klein, M.L., 1983. Comparison of simple potential functions for simulating liquid water. J. Chem. Phys. 79, 926–935.
Kabsch, W., Sander, C., 1984. On the use of sequence homologies to predict protein structure: identical pentapeptides can have completely different conformations. Proc. Natl. Acad. Sci. U.S.A. 81, 1075–1078.
Kaiser, E.T., Kezdy, F.J., 1987. Peptides with affinity for membranes. Annu. Rev. Biophys. Bio. Chem. 16, 561–581.
Koukos, P.I., Glykos, N.M., 2014. Folding molecular dynamics simulations accurately predict the effect of mutations on the stability and structure of a vammin-derived peptide. J. Phys. Chem. B. 118, 10076–10084.
Krebs, M.R., Domike, K.R., Donald, A.M., 2009. Protein aggregation: more than just fibrils. Biochem. Soc. Trans. 37, 682–686.
Krimm, S., Bandekar, J., 1986. Vibrational spectroscopy and conformation of peptides, polypeptides, and proteins. Adv. Prot. Chem. 38, 181–364.
Leslie, A.G.W., Powell, H.R., 2007. Processing Diffraction Data with Mosflm. Springer Netherlands, Dordrecht, The Netherlands.
Levy, E., Sastre, M., Kumar, A., Gallo, G., Piccardo, P., Ghetti, B., Tagliavini, F., 2001. Codeposition of cystatin C with amyloid-beta protein in the brain of Alzheimer disease patients. J. Neuropathol. Exp. Neurol. 60, 94–104.
Lindorff-Larsen, K., Piana, S., Palmo, K., Maragakis, P., Klepeis, J.L., Dror, R.O., Shaw, D.E., 2010. Improved side-chain torsion potentials for the Amber ff99SB protein force field. Proteins 78, 1950–1958.
Lopez de la Paz, M., Serrano, L., 2004. Sequence determinants of amyloid fibril formation. Proc. Natl. Acad. Sci. U.S.A. 101, 87–92.
Lopez, J., Martinez, A., 2002. Cell and molecular biology of the multifunctional peptide, adrenomedullin. Int. Rev. Cytol. 221, 1–92.
Luca, S., Yau, W.M., Leapman, R., Tycko, R., 2007. Peptide conformation and supramolecular organization in amylin fibrils: constraints from solid-state NMR. Biochemistry 46, 13505–13522.
Lynch, B., Kaiser, E.T., 1988. Biological properties of two models of calcitonin gene related peptide with idealized amphiphilic alpha-helices of different lengths. Biochemistry 27, 7600–7607.
Manning, M.C., 1989. Conformation of the alpha form of human calcitonin gene-related peptide (CGRP) in aqueous solution as determined by circular dichroism spectroscopy. Biochem. Biophys. Res. Commun. 160, 388–392.
McLatchie, L.M., Fraser, N.J., Main, M.J., Wise, A., Brown, J., Thompson, N., Solari, R., Lee, M.G., Foord, S.M., 1998. RAMPs regulate the transport and ligand specificity of the calcitonin-receptor-like receptor. Nature 393, 333–339.
Morales, R., Estrada, L.D., Diaz-Espinoza, R., Morales-Scheihing, D., Jara, M.C., Castilla, J., Soto, C., 2010. Molecular cross talk between misfolded proteins in animal models of Alzheimer's and prion diseases. J. Neurosci. 30, 4528–4535.
Morris, H.R., Panico, M., Etienne, T., Tippins, J., Girgis, S.I., MacIntyre, I., 1984. Isolation and characterization of human calcitonin gene-related peptide. Nature 308, 746–748.
Mossuto, M.F., Dhulesia, A., Devlin, G., Frare, E., Kumita, J.R., de Laureto, P.P., Dumoulin, M., Fontana, A., Dobson, C.M., Salvatella, X., 2010. The non-core regions of human lysozyme amyloid fibrils influence cytotoxicity. J. Mol. Biol. 402, 783–796.
Muff, R., Born, W., Fischer, J.A., 1995. Calcitonin, calcitonin gene-related peptide, adrenomedullin and amylin: homologous peptides, separate receptors and overlapping biological actions. Eur. J. Endocrinol. 133, 17–20.
Nanga, R.P., Brender, J.R., Vivekanandan, S., Ramamoorthy, A., 2011. Structure and membrane orientation of IAPP in its natively amidated form at physiological pH in a membrane environment. Biochim. Biophys. Acta 1808, 2337–2342.
Nelson, R., Eisenberg, D., 2006. Structural models of amyloid-like fibrils. Adv. Protein Chem. 73, 235–282.
Ogoshi, M., Inoue, K., Naruse, K., Takei, Y., 2006. Evolutionary history of the calcitonin gene-related peptide family in vertebrates revealed by comparative genomic analyses. Peptides 27, 3154–3164.
Paravastu, A.K., Leapman, R.D., Yau, W.M., Tycko, R., 2008. Molecular structural basis for polymorphism in Alzheimer's beta-amyloid fibrils. Proc. Natl. Acad. Sci. U.S.A. 105, 18349–18354.
Portaluppi, F., Vergnani, L., Margutti, A., Ambrosio, M.R., Bondanelli, M., Trasforini, G., Rossi, R., Degli Uberti, E.C., 1993. Modulatory effect of the renin-angiotensin system on the plasma levels of calcitonin gene-related peptide in normal man. J. Clin. Endocrinol. Metab. 77, 816–820.
Poyner, D.R., Tomlinson, A.E., Gosling, M., Tough, I.R., Cox, H.M., 1993. Stimulation of chloride secretion and adenylate cyclase secretion in human colonic derived cell lines by calcitonin gene-related peptide. Biochem. Soc. Trans. 21, 434S.
Poyner, D.R., Taylor, G.M., Tomlinson, A.E., Richardson, A.G., Smith, D.M., 1999. Characterization of receptors for calcitonin gene-related peptide and adrenomedullin on the guinea-pig vas deferens. Br. J. Pharmacol. 126, 1276–1282.
Poyner, D.R., Sexton, P.M., Marshall, I., Smith, D.M., Quirion, R., Born, W., Muff, R., Fischer, J.A., Foord, S.M., 2002. International Union of Pharmacology. XXXII. The mammalian calcitonin gene-related peptides, adrenomedullin, amylin, and calcitonin receptors. Pharmacol. Rev. 54, 233–246.
Preibisz, J.J., 1993. Calcitonin gene-related peptide and regulation of human cardiovascular homeostasis. Am. J. Hypertens. 6, 434–450.
Reches, M., Porat, Y., Gazit, E., 2002. Amyloid fibril formation by pentapeptide and tetrapeptide fragments of human calcitonin. J. Biol. Chem. 277, 35475–35480.
Roberts, A.N., Leighton, B., Todd, J.A., Cockburn, D., Schofield, P.N., Sutton, R., Holt, S., Boyd, Y., Day, A.J., Foot, E.A., et al., 1989. Molecular and functional characterization of amylin, a peptide associated with type 2 diabetes mellitus. Proc. Natl. Acad. Sci. U.S.A. 86, 9662–9666.
Rocken, C., Sletten, K., 2003. Amyloid in surgical pathology. Virchows Arch. 443, 3–16.
Romhanyi, G., 1971. Selective differentiation between amyloid and connective tissue structures based on the collagen specific topo-optical staining reaction with congo red. Virchows Archiv. A: Pathol. Pathologische Anatomie 354, 209–222.
Rosenfeld, M.G., Emeson, R.B., Yeakley, J.M., Merillat, N., Hedjran, F., Lenz, J., Delsert, C., 1992. Calcitonin gene-related peptide: a neuropeptide generated as a consequence of tissue-specific, developmentally regulated alternative RNA processing events. Ann. N.Y Acad. Sci. 657, 1–17.
Russell, F.A., King, R., Smillie, S.J., Kodji, X., Brain, S.D., 2014. Calcitonin gene-related peptide: physiology and pathophysiology. Physiol. Rev. 94, 1099–1142.
Salomon-Ferrer, R., Case, D.A., Walker, R.C., 2013. An overview of the Amber biomolecular simulation package. Wiley Interdiscip. Rev.: Comput. Mol. Sci. 3, 198–210.
Shivu, B., Seshadri, S., Li, J., Oberg, K.A., Uversky, V.N., Fink, A.L., 2013. Distinct beta-sheet structure in protein aggregates determined by ATR-FTIR spectroscopy. Biochemistry 52, 5176–5183.
Sievers, F., Wilm, A., Dineen, D., Gibson, T.J., Karplus, K., Li, W., Lopez, R., McWilliam, H., Remmert, M., Soding, J., Thompson, J.D., Higgins, D.G., 2011. Fast, scalable generation of high-quality protein multiple sequence alignments using Clustal Omega. Mol. Syst. Biol. 7, 539.
Sipe, J.D., Benson, M.D., Buxbaum, J.N., Ikeda, S.I., Merlini, G., Saraiva, M.J., Westermark, P., 2016. Amyloid fibril proteins and amyloidosis: chemical identification and clinical classification International Society of Amyloidosis 2016 Nomenclature Guidelines. Amyloid: Int. J. Experim. Clin. Invest. 23, 209–213.
Smaoui, M.R., Poitevin, F., Delarue, M., Koehl, P., Orland, H., Waldispuhl, J., 2013. Computational assembly of polymorphic amyloid fibrils reveals stable aggregates. Biophys. J. 104, 683–693.
Somavarapu, A.K., Kepp, K.P., 2015. The dependence of amyloid-beta dynamics on

protein force fields and water models. Chemphyschem: A Eur. J. Chem. Phys. Phys. Chem. 16, 3278–3289.
Sunde, M., Blake, C., 1997. The structure of amyloid fibrils by electron microscopy and X-ray diffraction. Adv. Protein. Chem. 50, 123–159.
Surewicz, W.K., Mantsch, H.H., Chapman, D., 1993. Determination of protein secondary structure by Fourier transform infrared spectroscopy: a critical assessment. Biochemistry 32, 389–394.
Tsigelny, I.F., Crews, L., Desplats, P., Shaked, G.M., Sharikov, Y., Mizuno, H., Spencer, B., Rockenstein, E., Trejo, M., Platoshyn, O., Yuan, J.X., Masliah, E., 2008. Mechanisms of hybrid oligomer formation in the pathogenesis of combined Alzheimer's and Parkinson's diseases. PloS One 3, e3135.
Tsiolaki, P.L., Louros, N.N., Hamodrakas, S.J., Iconomidou, V.A., 2015. Exploring the 'aggregation-prone' core of human Cystatin C: a structural study. J. Struct. Biol. 191, 272–280.
Tycko, R., 2015. Amyloid polymorphism: structural basis and neurobiological relevance. Neuron 86, 632–645.
Ulbrich, L., Cozzolino, M., Marini, E.S., Amori, I., De Jaco, A., Carri, M.T., Augusti-Tocco, G., 2014. Cystatin B and SOD1: protein-protein interaction and possible relation to neurodegeneration. Cell Mol. Neurobiol. 34, 205–213.
Uversky, V.N., Fink, A.L., 2004. Conformational constraints for amyloid fibrillation: the importance of being unfolded. Biochim. Biophys. Acta 1698, 131–153.
Valenti, L.E., Paci, M.B., De Pauli, C.P., Giacomelli, C.E., 2011. Infrared study of trifluoroacetic acid unpurified synthetic peptides in aqueous solution: trifluoroacetic acid removal and band assignment. Anal. Biochem. 410, 118–123.
Van Der Spoel, D., Lindahl, E., Hess, B., Groenhof, G., Mark, A.E., Berendsen, H.J., 2005. GROMACS: fast, flexible, and free. J. Comput. Chem. 26, 1701–1718.
Vega, A.V., Avila, G., 2010. CGRP, a vasodilator neuropeptide that stimulates neuromuscular transmission and EC coupling. Curr. Vasc. Pharmacol. 8, 394–403.
Waterhouse, A.M., Procter, J.B., Martin, D.M., Clamp, M., Barton, G.J., 2009. Jalview Version 2–a multiple sequence alignment editor and analysis workbench. Bioinformatics 25, 1189–1191.
Westermark, G.T., Westermark, P., 2008. Transthyretin and amyloid in the islets of Langerhans in type-2 diabetes. Exp. Diabetes Res. 2008, 429274.
Westermark, P., Wernstedt, C., Wilander, E., Sletten, K., 1986. A novel peptide in the calcitonin gene related peptide family as an amyloid fibril protein in the endocrine pancreas. Biochem. Biophys. Res. Commun. 140, 827–831.
Westermark, P., Engstrom, U., Johnson, K.H., Westermark, G.T., Betsholtz, C., 1990. Islet amyloid polypeptide: pinpointing amino acid residues linked to amyloid fibril formation. Proc. Natl. Acad. Sci. U.S.A. 87, 5036–5040.
Wetzel, R., Shivaprasad, S., Williams, A.D., 2007. Plasticity of amyloid fibrils. Biochemistry 46, 1–10.
Wiltzius, J.J., Sievers, S.A., Sawaya, M.R., Cascio, D., Popov, D., Riekel, C., Eisenberg, D., 2008. Atomic structure of the cross-beta spine of islet amyloid polypeptide (amylin). Protein Sci. 17, 1467–1474.
Wimalawansa, S.J., 1997. Amylin, calcitonin gene-related peptide, calcitonin, and adrenomedullin: a peptide superfamily. Crit. Rev. Neurobiol. 11, 167–239.
Yan, J., Fu, X., Ge, F., Zhang, B., Yao, J., Zhang, H., Qian, J., Tomozawa, H., Naiki, H., Sawashita, J., Mori, M., Higuchi, K., 2007. Cross-seeding and cross-competition in mouse apolipoprotein A-II amyloid fibrils and protein A amyloid fibrils. Am. J. Pathol. 171, 172–180.
Zhang, Z., Chen, H., Bai, H., Lai, L., 2007. Molecular dynamics simulations on the oligomer-formation process of the GNNQQNY peptide from yeast prion protein Sup35. Biophys. J. 93, 1484–1492.